Computers and Concrete, *Vol. 36, No. 2 (2025) 199-216*
https://doi.org/10.12989/cac.2025.36.2.199

Mechanical properties of concrete produced with recycled fiber formed waste tire rubber and prediction of capacity with various approaches

Ali Serdar Ecemiş[1], Şaban Gülcü[2], Emrah Madenci*[1,3], Ali İhsan Çelik[4] and Yasin Onuralp Özkılıç**[1]

[1]*Necmettin Erbakan University, Faculty of Engineering, Department of Civil Engineering, Konya, Türkiye*
[2]*Necmettin Erbakan University, Faculty of Engineering, Department of Computer Engineering, Konya, Türkiye*
[3]*Department of Technical Sciences, Western Caspian University, Baku 1001, Azerbaijan*
[4]*Tomarza Mustafa Akincioglu Vocational School, Department of Construction, Kayseri University, Kayseri, 38940, Türkiye*

(*Received May 1, 2023, Revised May 2, 2023, Accepted February 23, 2025*)

Abstract. This paper investigates the compressive, tensile, and flexural behavior of concrete produced using waste tire rubber in the form of fibers, and also estimates its capacities with artificial neural networks (ANN). This study aims to reuse waste tires in concrete production by considering environmental awareness and recycling, both of which are becoming increasingly important. Three different ratios of fiber-formed waste tire rubber, specifically 5%, 10%, and 15% by volume, were utilized. Slump value measurement, compressive strength, splitting tensile strength, and flexural tests were performed on the samples. The distribution of rubber fibers in the concrete was investigated by SEM. Thanks to the developed algorithm, ANN was performed, and the optimum design configuration was determined. When the results of the analysis were examined, it was observed that the use of waste rubber in the form of fiber increased the workability of the concrete, while it caused a decrease in the compressive strength, cylinder splitting strength, and beam bending tensile strength . As the ratio of tires used increases, the more the reduction in these strengths becomes pronounced.

Keywords: fiber composite concrete; mechanical tests; recycled tire rubber-filled concrete; rubber

1. Introduction

Concrete technology is developing rapidly . Within the framework of this development, many properties of concrete are being improved. Many researchers have used solid waste in concrete components (cement, water, aggregates, mineral and chemical additives) especially instead of aggregates. Thus, methods were sought to evaluate these wastes, which cause environmental pollution. A waste tire is one of the biggest waste materials that threatens the environment and health, poses a fire hazard, and is costly to dispose of (Elchalakani *et al.* 2016). The management and disposal of waste tires is an important environmental issue that is difficult to address (Elchalakani 2015). One practical way to reuse such industrial waste is to include used tires in cement-based products, particularly concrete, which comprises the bulk of building materials (Han *et al.* 2015, 2016).

Rubberized Concrete (RuC) is made by mixing tires with cement, thus protecting natural resources and reducing the number of tires dumped in landfills. The reuse of tires, in small parts such as rubber pieces, in cement-containing products like asphalt, filler, rubber sheets, or concrete, has been the subject of several studies during the past 20 years. Applications for recycling small tires have been extensively researched, particularly in concrete pavement blocks, waterproofing systems, and membrane fillers (Ke *et al.* 2022, Habib and Yildirim 2021). Due to its low unit weight, concrete containing rubber aggregate is commonly used for sound barriers, roadsides, and pavement. To save the environment, shredded waste tires have recently been assessed in the building industry.

Research on structural elements shows that using recycled tire aggregate instead of natural aggregate produces structural elements that behave better, including greater ductility, than concrete made with conventional aggregates. The disadvantages of adding extra rubber to concrete include a decline in elastic modulus and a reduction in compressive and tensile strength. According to studies, substituting rubber for natural aggregates in concrete, reduces workability. The grain size of the rubber and the percentage of rubber used in producing concrete are the main factors influencing workability (Bisht and Ramana 2017). Examples of these experiments include the utilization of rubber granules as aggregate in concrete, and the creation of crash barriers using this concrete. According to certain research, waste tire aggregate has a lower unit density than conventional aggregate, reducing the unit density of concrete. It has been claimed that lightweight concrete can be made by adding 20% or around 60% of tire aggregate, due to the low unit densities of concrete containing rubber aggregates. These two concentrations imply different resultant properties.

*Corresponding author, Associate Professor
E-mail: emandenci@erbakan.edu.tr
**Corresponding author, Associate Professor
E-mail: yozkilic@erbakan.edu.tr

Copyright © 2025 Techno-Press, Ltd.

ISSN: 1598-8198 (Print), 1598-818X (Online)

A concrete type known as rubberized concrete (RuC) has undergone extensive study over the past three decades and has emerged as a useful alternative for use in structural components, including concrete beams, columns, and railway sleepers where energy dissipation and ductility are crucial criteria. Rubber aggregates recycled from used tires (by volume or by weight) are used in RuC to partially replace natural fine and coarse aggregates. Rubber aggregates are less dense than natural aggregates, so RuC is less dense than conventional concrete. When compared to regular concrete, RuC lowers the inherent frequency of the structural components, and increases damping ratio values. Increased rubber concentration in concrete results in a further loss of workability, regardless of rubber size (0-20 mm).

The assessment of the RuC physical and mechanical properties (Toutanji 1996), microstructure characteristics (Navarro *et al.* 2005), dynamic performance (Zheng *et al.* 2008), energy dissipation capacity (Hernandez-Olivares *et al.* 2002), durability (Topçu and Demir 2007), and industrial applications was the main area of study. The majority of RuC-related studies examined the material-level impact of rubber in concrete. Typically, a concrete mix is used in these tests, and several RuC mixtures are made by adding various amounts of crumbed rubber and proportionately reducing the fine aggregate in the original mix. The mechanical characteristics of the reactive ultra-high-strength concrete (RuCs) are compared to those of regular concrete. According to Khaloo *et al.* (2008), replacing fine aggregate with smaller rubber particles resulted in the greatest compression strength and elasticity loss, whereas replacing coarse aggregate resulted in the most significant loss. Ganjian *et al.* (2009) replaced 5-10% of the cement in concrete with rubber powder, which led to a drop in the material's compressive strength as well as the elasticity modulus. A study on low-volume rubberized concrete was conducted by Li *et al.* (2014). According to Liu *et al.* (2013), the ratio of RuCs flexural strength to compressive strength rises, in comparison to regular concrete, demonstrating that the rubber performs better against cracking. In addition, they discovered that increasing the rubber volume concentration boosts the concrete's hardness.

Resistance to impact load can increase as the rubber particle ratio increases up to a maximum of 50% replacement, but it has been determined that the impact resistance decreases with further growth in rubber content (Reda Taha *et al.* 2008). Rubber particles are incorporated into concrete to minimize its thermal expansion and contraction and to bridge microcracks caused by exposure to high temperatures. The bonding behavior of the cement mix is the main factor that generally causes RC to have poor mechanical performance. Increased rubber content reduces concrete density and increases concrete porosity, which significantly reduces mechanical strength. Since a number of factors influence how well the RC performs, it is essential to discuss the impact of those elements in a single study (Bušić *et al.* 2018).

Rubber with a denser grain size has a greater negative effect on the strength of composites than one with a finer grain size, due to the weak mechanical properties of rubber. Smaller rubber particles fill the matrix's pores, creating a more compact matrix that increases the matrix's compressive strength (Su *et al.* 2015). Stallings *et al.* (2019) conducted research to determine how the replacement of rubber coarse aggregate affected the compressive strength of concrete. The only reference used was the compressive strength of a sample entirely composed of natural aggregates. The results showed that thinner rubber enhanced compressive strength at lower replacement ratios, but thicker rubber caused a considerable drop at all replacement ratios. The inclusion of aggregates with 19 mm particle size decreased compressive strength relative to the reference sample by around 28.6%, 48.6%, 65.7%, and 74.3% for 10%, 20%, 30%, and 40% content levels, respectively. Concrete offers many useful mechanical qualities, even though the presence of rubber parts seems to reduce these qualities. As an illustration, it has been demonstrated that adding rubber to concrete in a proportion of around 30% by weight of cement enhances non-structural fracture resistance, shock wave absorption, and acid resistance, while decreasing thermal conductivity and sound level. Additionally, rubberized concrete has a density that is around 22% lower than ordinary concrete, making it lighter.

Artificial Neural Network (ANN) models can accurately predict their mechanical properties, as they can capture the complex interrelations among various factors affecting RuC performance, including rubber content, concrete mix design, and associated curing conditions. The prediction capability provided by ANNs can be very useful in optimizing RuC mix design and performance, which is essential for the real-world application of this material within the construction industry.

Some research in the civil engineering area had already been done on artificial intelligence techniques to create a model and to control the model's different parameters. ANN is one of the techniques in artificial intelligence. ANN is known for being an intelligent method for modeling the behavior of physical phenomena. Saving time and money, ANN finds answers by using data samples instead of whole data sets. ANN is modeled after the human brain. The capabilities of the human brain are modeled after by artificial neural networks (ANNs). Learning allows the generation, production, and discovery of new knowledge (Gülcü 2020). In civil engineering, waste tires are added to cement. Thus, waste tires are recycled and the strength of the concrete is increased. However, the compressive strength of rubberized concrete varies according to the amount of substances added to it. To find the optimum compressive strength, the amount of substances added is empirically determined. ANN has been used to solve these problems in the civil engineering field. For instance, the DA-MLP (Gülcü 2022a) and IAMO-MLP (Gülcü 2022b) algorithms based on ANN were developed and used to predict the compressive strength. The aim of the ANN in this study is to develop three models that can accurately predict. The models predict compressive stress, the splitting tensile stress, and the flexure stress. The models are built using four input parameters. Furthermore, the data set used by ANN was gathered from the literature. The ANN formulation generates models that have physical reality.

Table 1 Mix proportions

#	Coarse Aggregate (kg)				Fine Aggregate (kg)			Cement (C) kg/m^3	Water (W) kg/m^3	W/C	Super Plasticizer kg	Unit Weight kg/m^3
	4-11.2 mm	11.2-22.4 mm	Rubber (%)	Rubber (kg)	0-4 mm	Rubber (%)	Rubber (kg)					
RNC	328.15	483.59	0.00	0.00	1107.26	0.00	0.00	270	186.30	0.69	1.080	2376
RuNC - %5	311.74	459.41	5	16.27	1051.90	5	19.78	270	186.30	0.69	1.080	2316
RuNC - %10	295.34	435.23	10	32.53	996.54	10	39.56	270	186.30	0.69	1.080	2257
RuNC - %15	278.93	411.05	15	48.80	941.17	15	59.34	270	186.30	0.69	1.080	2197



Fig. 1 Test samples production

In this regard, the purpose of this work is to experimentally explore the behavior of concrete produced with rubber derived from waste tires. The parameters examined are four rubber replacement rates, 0%, 5%, 10%, and 15% by volume of the fine and coarse aggregates. Fresh and hardened properties of the rubberized concrete were examined. In literature, most studies were focused on crumb types of waste rubber. In this study, the effect of fiber-formed rubber produced from waste tires on the behavior of concrete is examined. Furthermore, a comprehensive data set was collected to train the ANN to predict the capacities of the waste rubber.



Fig. 2 Produced samples

2. Experimental program

In addition to the reference sample, the test set consists of a mixture of 3 different fiber formed waste tire rubber ratios. All specimens were produced in the laboratories of Necmettin Erbakan University Civil Engineering Department. Tire ratios used in the mixture were chosen as 5%, 10%, and 15% by volume. Three of each mixture were produced and put to the test.

2.1 Material properties of rubberized concrete (RuC)

Waste tires can be prepared for use as aggregate in concrete by applying various cutting and grinding methods. According to the method of cutting and chopping, and their usage of use, waste tires are classified as scrap, torn, chip-shaped, ground, and crumb. The ratio of waste rubber in fiber form to be used in the research was determined to be 5%, 10%, and 15% by volume. Concrete mixing ratios are provided in Table 1, and the production of samples and the test samples are shown in Figs. 1 and 2, respectively. In Table 1, RNC refers to reference normal concrete, RuNCi refers to rubberized normal concrete, and % refers to the proportion of rubber used in the mix by volume.

First, coarse and light aggregate (fiber-formed rubber, if used) was added to the mixer. Super-plasticizer and approximately 1/3 of the calculated amount of water were added and mixed for 1 minute. In the next stage, fine aggregate, cement, and the remaining two-thirds of the water were added and mixed for three more minutes. After this stage, a resting period of 3 minutes was observed, and then the concrete production was completed, with an additional 2 minutes of mixing. Care was taken to avoid segregation during production and placement (ASTM C 192/C 192M-02 2002). Aggregate used in the experiments was obtained from the Konya region. Fine aggregate (0-4 mm) and coarse aggregate in two different sizes (4-11.2



Fig. 3 Waste tire rubber fiber forms

Table 2 Properties of cement

Chemical Properties	Values	TS EN 197-1	
		Min.	Max.
Glow Loss (%)	4.36		5.00
Insoluble Residue (%)	0.50		5.00
Sulfur Trioxide (SO3) (%)	3.53		4.00
Chloride (Cl) (%)	0.021		0.10
K2O (%)	0.64		
Na2O (%)	0.32		
Physical Properties	**Values**	**TS EN 197-1**	
		Min	Max
Specific Surface (cm^2/gr)	3758		
2 Day Compressive Strength (MPa)	25.58	20.0	
28 Day Compressive Strength (MPa)	47.1	42.5	62.5
Concrete Setting Start (min.)	161	60	
Volume Expansion (mm)	2		10

mm) and (11.2-22.4 mm) were used.

Fiber-form waste tire rubber was selected for the study, sifted , separated into fine fiber and coarse fiber according to their size. The classification was determined as:

i) Coarse fiber rubber aggregates passing through 16 mm sieve and remaining on 4 mm sieve

ii) Fine fiber rubber aggregates passing through 4 mm sieve.

The rubber forms used are shown in Fig. 3.

To obtain high strength in the study, CEM I 42.5 R cement, produced by Konya Cement, was used. The physical and chemical properties of the cement produced according to TS-EN 197-1 are given in Table 2.

Politon 612, a polycarboxylate-based super plasticizer concrete additive that reduces the mixing water in concrete, increases strength, and improves the workability of fresh concrete, was used in the study. The limit values for the effect of this superplasticizer additive on the performance of concrete, are in compliance with those given in TS EN 934-2 and ASTM C 494 standards.



Fig. 4 Compressive test

2.2 Compressive test

The cube specimens produced were subjected to the pressure test. The loading rate is 680 kgf/s. Compressive strength tests were carried out in accordance with TS EN 12390-3 and TS EN 12390-4. For the reference sample selected as an example, the experimental setup is shown in Fig. 4.



Fig. 5 Splitting test



Fig. 6 Flexure test

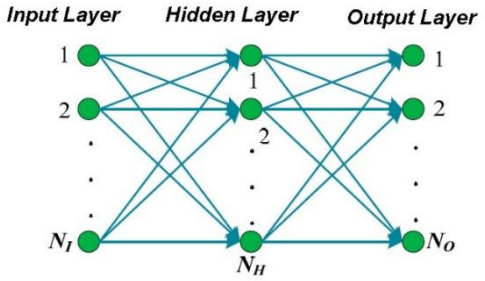


Fig. 7 The general structure of the FFNN

2.3 Splitting tensile test

Cylindrical specimens were subjected to a splitting test. The loading speed is 240 kgf/s. Cylinder splitting strength tests were carried out according to TS EN 12390-6. Fig. 5 shows the experimental setup, using the reference specimen as an example.

2.4 Flexure test

Produced samples were tested under three-point loading. Flexural strength tests were carried out using the two-point loading method according to TS EN 12390-5. The experimental setup is shown in Fig. 6 for the reference sample chosen for illustration.

3. Artificial neural network (ANN) analysis

A computer system called an artificial neural network (ANN) is modeled after the human brain. The capabilities of the human brain are automatically emulated by ANN. Learning allows individuals or systems to generate and find new knowledge. An ANN is a mathematical model that simulates the learning processes of a neural network. Artificial networks or systems imitate the structure of organic brain networks to facilitate learning, recollection, and generalization. ANNs use instance data sets to aid in their learning process. When input and output data are provided during the learning process, patterns can be generated (Gülcü 2020). The most widely used model of these is the feed-forward neural network (FFNN) (Gülcü 2022). FFNN offers many benefits. Numerous units that make up the FFNN operate concurrently and carry out intricate functions. can use a variety of learning techniques. FFNN can create classifications, perform pattern recognition, as well as generate insights for unseen outputs. FFNN can use incomplete or ambiguous information and fill in missing patterns. FFNN can analyze real-time data and operate in parallel.

Neurons are data-processing components that make up a feedforward neural network. The input layer sends data to the neurons, which translate it for the network. The network's findings are provided through the output layer. Between the input layer and the output layer lies the hidden layer. Weights are the links that allow neurons to connect to one another. Calculating the values of the weights that the model will use to provide the best score is fundamental to FFNN. Fig. 7 depicts the FFNN's general structure.

The outputs of neurons in a layer pass through the weights to become inputs to the neurons in the following layer. Information in the network is transferred in one direction from the input layer to the output layer. The performance of FFNN depends on updating the network with optimum values of the biases and weights. The output of each neuron is calculated by the function shown in Eqs. (1) and (2).

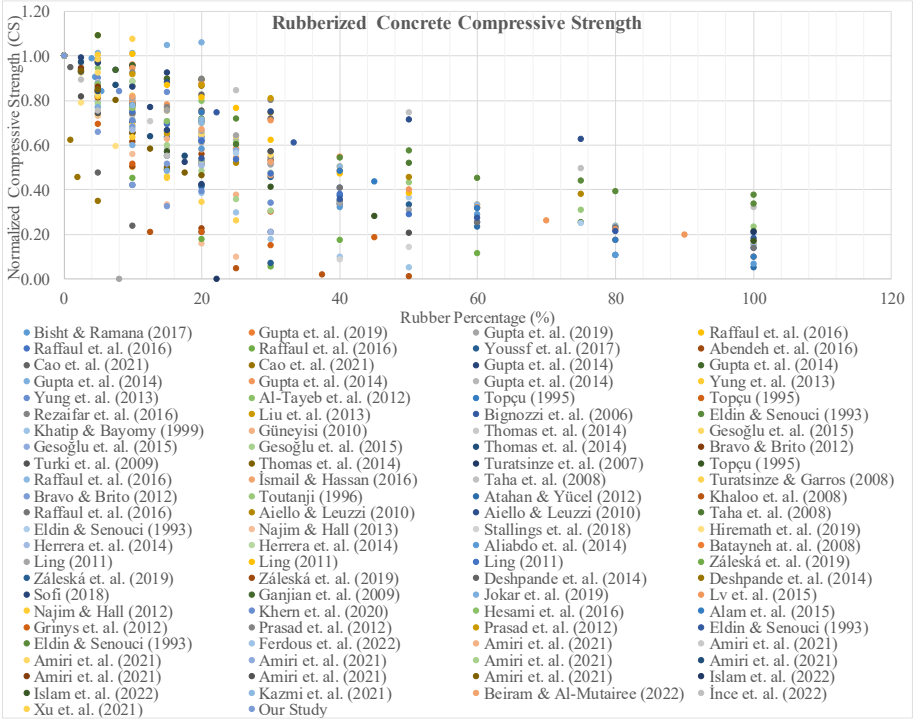


Fig. 8 Rubberized concrete compressive strength

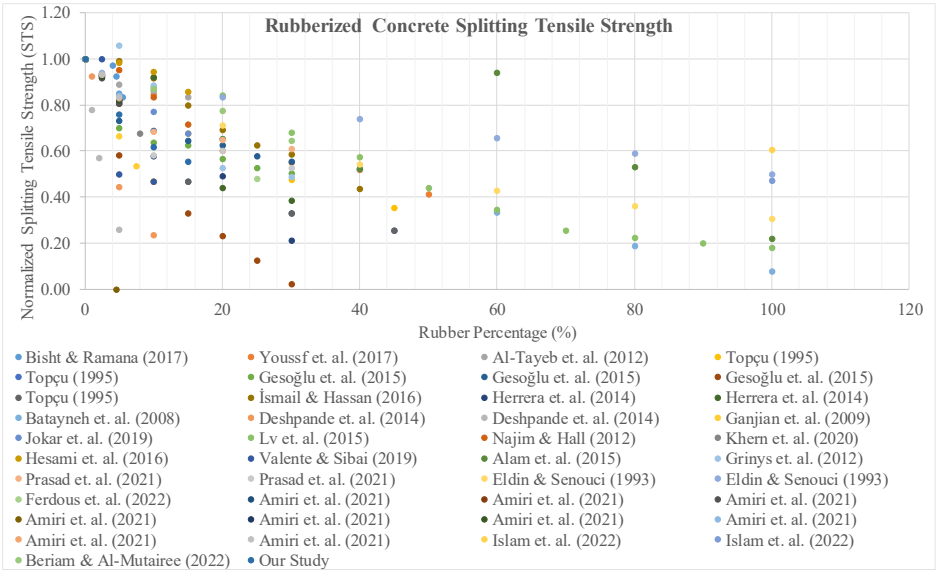


Fig. 9 Rubberized concrete splitting tensile strength

$$T_i = Sigmoid(t_i) = \frac{1}{1+e^{-t_i}} \quad (1)$$

$$t_i = \sum_{k=1}^{m}(A_{ki} * G_k) - \beta_i\,,\ i = 1,2,\dots,n \quad (2)$$

Where m, n, k, and i represent the total number of neurons in the layer, the total number of neurons in the next layer, a neuron in the layer, and a neuron in the next layer, respectively. A_{ki} represents the weight between the kth neuron in the layer and the ith neuron in the next layer. G_k represents the input data. β_i represents the bias value of the ith neuron in the next layer.

In general, the input dataset in FFNN is randomly split into the training dataset, the validation dataset, and the test dataset. We used the training data, validation data, and test data as 70%, 15%, and 15% of the input dataset, respectively. In addition, all data sets are normalized by the function in Eq. (3). The effects on the results of attributes that can have varied rates are eliminated (Gülcü 2022).

$$x' = \frac{(x-x_{min})}{(x_{max}-x_{min})} \quad (3)$$

where x' represents the normalized form of x.

The values of the biases and weights are randomly initialized at the beginning of the algorithm and affect the performance of the FFNN. They are randomly initialized

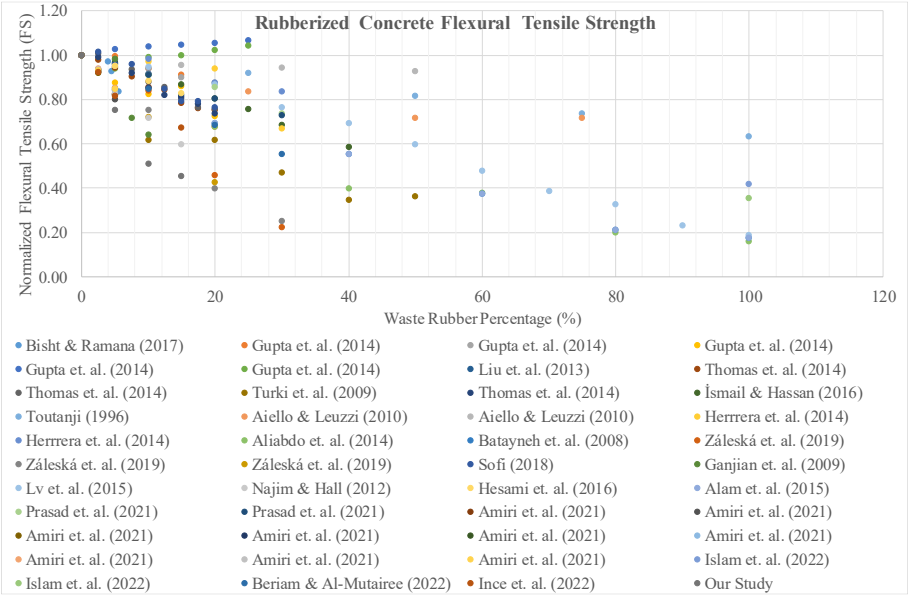


Fig. 10 Rubberized concrete flexural tensile strength

between -1 and 1 in this study. The weights and biases of FFNN are optimized in accordance with the input-output pattern in the training dataset. In this study, the mean square error (MSE) was used as the objective function, and its formulation is given in Eq. (4). The aim is to minimize the MSE. In this study, to find the best FFNN model, the number of neurons in the hidden layer started from 2, and then increased by one up to 30. Therefore, 29 FFNN architectures were used to determine the best model. These architectures look like 4-2-1, 4-3-1, …, 4-30-1. At the end of the training network phase, we create 29 models with the minimum MSE. The validation dataset is successively applied to each of the 29 models. Thus, the best model among the models is found, according to the minimum MSE. Finally, the test dataset is used to provide an unbiased evaluation of the best model fit on the training dataset. Thus, the best model is ready to use.

To assess the performance of FFNN, the statistical metrics, which are frequently used in literature, were applied. These statistical metrics are the MSE, the correlation coefficient (R), and the mean absolute error (MAE). Their formulations are shown in Eqs. (4)-(6).

$$MSE = (\sum_{i=1}^{N}(O_i - P_i)^2)/N \quad (4)$$

$$MAE = (\sum_{i=1}^{N}|O_i - P_i|)/N \quad (5)$$

$$R = \sqrt{1 - (\sum_{i=1}^{N}(O_i - P_i)^2/\sum_{i=1}^{N}(O_i - \bar{P})^2)} \quad (6)$$

where N, O, P, and $\bar{P}$ are the number of instances in the dataset, the observed value, the predicted value, and the mean of the predicted values, respectively.

In the study, the compressive strengths, cylinder splitting strengths, and bending tensile strengths of concretes produced using waste rubber at different rates, as obtained from the literature review, were used as the data set of the ANN (Bignozzi and Sandrolini 2006, Turatsinze *et al.* 2007, Batayneh *et al.* 2008, Khaloo *et al.* 2008, Reda *et al.* 2008, Turatsinze and Garros 2008, Ganjian *et al.* 2009, Güneyisi 2009, Turki *et al.* 2009, Aiello and Leuzzi 2010, Ling 2011, Al-Tayeb *et al.* 2012, Atahan and Yücel 2012, Bravo and de Brito 2012, Grinys *et al.* 2012, Najim and Hall 2012, Liu *et al.* 2013, Najim and Hall 2013, Yung *et al.* 2013, Gupta *et al.* 2014, Herrera-Sosa *et al.* 2014, Thomas *et al.* 2014, Aliabdo *et al.* 2015, Gesoglu *et al.* 2015, Lv *et al.* 2015, Abendeh *et al.* 2016, Hesami *et al.* 2016, Ismail and Hassan 2016, Raffoul *et al.* 2016, Rezaifar *et al.* 2016, Bisht and Ramana 2017, Youssf *et al.* 2017, Sofi 2018, Stallings *et al.* 2018, Gupta *et al.* 2019, Jokar *et al.* 2019, Valente and Sibai 2019, Záleská *et al.* 2019, Khern *et al.* 2020, Roychand *et al.* 2020, Amiri *et al.* 2021, Cao *et al.* 2021, Ferdous *et al.* 2021, Guru Prasad *et al.* 2021, Kazmi *et al.* 2021, Xu *et al.* 2021, Beiram and Al-Mutairee 2022, Ahmad *et al.* 2022, Ince *et al.* 2022, Islam *et al.* 2022). The data used in this approach are shown in Figs. 8-10 for compressive strength, tensile splitting strength and flexural strength, respectively.

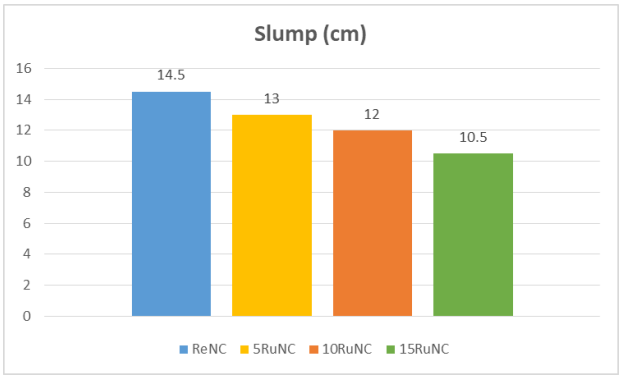


Fig. 11 Slump values

4. Results

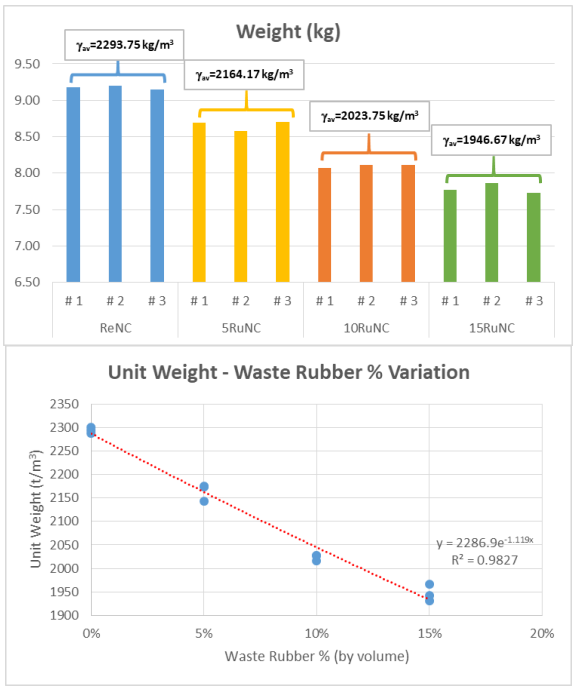


Fig. 12 The unit weight of the concrete

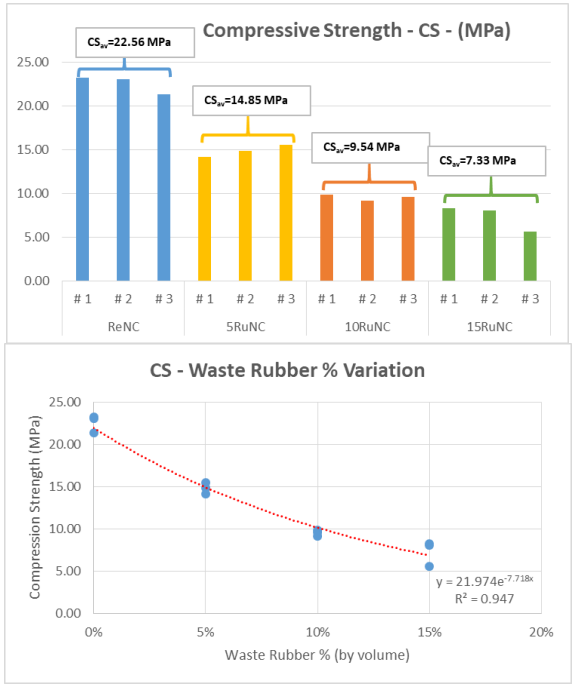


Fig. 13 The compressive strength of concrete

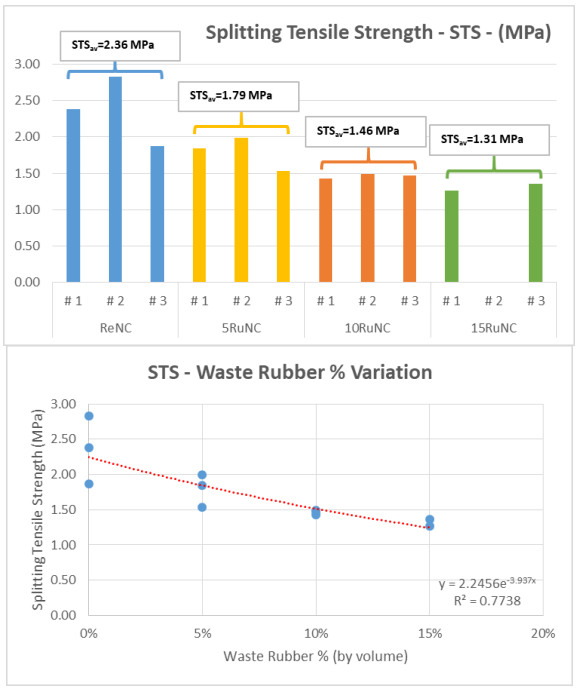


Fig. 14 The cylinder splitting strength

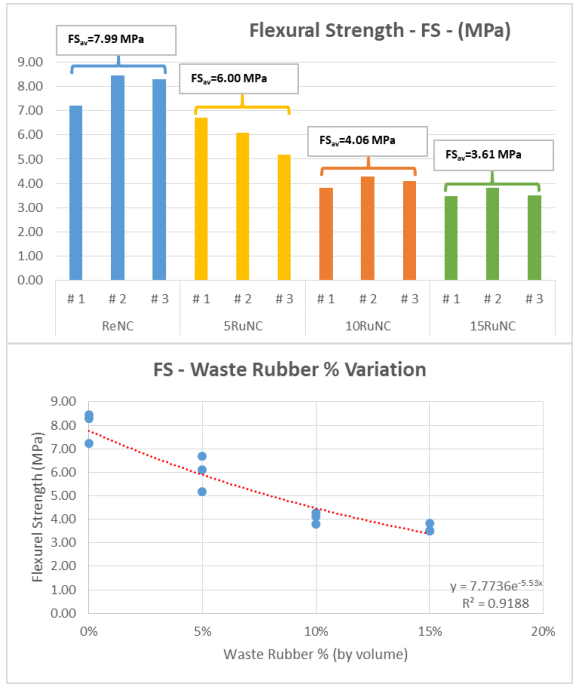


Fig. 15 The flexure strength

In this study, experiments were carried out on cube, cylinder, and beam samples containing waste tire rubber in the form of fiber at ratios of 5/10/15% by volume, and the slump values of the prepared composite concrete mixture were examined. In the study, the water/cement ratio was kept constant as 0.69.

4.1 Mechanical test results

The slump values decreased compared to the reference specimen when the tire ratio rose (Fig. 11). The tire ratio was increased, which improved workability. This is because, although the water/cement ratio is maintained and the tire's water absorption is low due to rubber, an increase in reacting water causes the mixture's consistency to become more fluid and reduces its internal friction coefficient.

The unit weight of the concrete has decreased due to using rubber instead of aggregate because the tire is lower in unit weight than the aggregate (Fig. 12). The rate of reduction also increased with the amount of rubber used. Compared to the reference sample, this drop is around

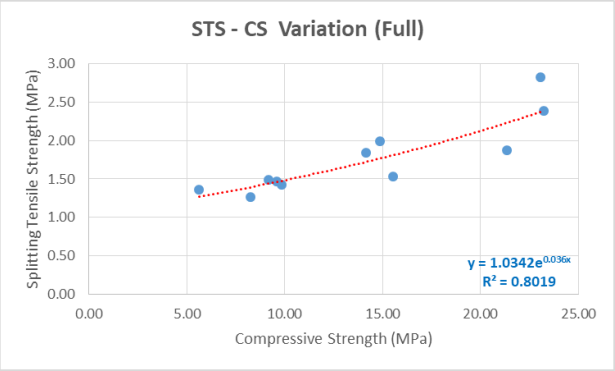


Fig. 16 Splitting tensile strength-Compressive strength variation

5.6%, 12%, and 15%. It can be argued that when the tire is utilized by volume, there is a drop in unit volume weight, approximately equal to the ratio of the tire used, but it varies depending on the physical features of the tire used in the mixture.

The most important property sought in concrete is compressive strength. Rubber's low compressive strength and the structure's compressibility, and flexibility result in a reduction in concrete's compressive strength (Fig. 13). Considering the compressive strength, which is its key physical property and the primary reason for its use, this decrease is undesirable. However, the rate of decrease in the compressive strength of rubberized concrete increases as the rubber ratio used increases. Depending on the tire ratio employed, this drop is around 66%, 42%, or 32.5% of the reference sample, respectively, when the analytical results are evaluated,. This result shows that if rubberized concrete is used in a structural design, it would be advisable to use innovative concrete production methods to provide the necessary compressive strength.

A material like concrete can exhibit low shear strength under certain conditions. In a typical concrete mix, the shear strength ranges from around 35% to 80% of the compressive strength. The tensile strength is only around 10% of the compressive strength, indicating a significant difference. According to the cylinder split test and the Boussinesq equation based on the theory of elasticity, the concrete's tensile strength was determined as described by Eq. (7), where "*P*" is the splitting load, "*d*" is the cylinder diameter, and "*l*" is the cylinder length.

$$\sigma_x = f_{cts} = \frac{2P}{\pi dl} \tag{7}$$

The results of the testing, revealed that the splitting tensile strength of the reference sample's cylinder was 2.36 MPa (Fig. 14). In parallel with the use of waste tires, this study examines a decrease in the splitting tensile strength of concrete, as well as in other properties of concrete. Depending on the rubber ratio employed, this drop is around 76 percent, 62 percent, or 55.5 percent of the reference sample. The results of the cylinder splitting test showed a decline, albeit not as much as the decline of the compressive strength.

The bending tensile strength, assuming Hooke's law is valid,

Table 3 Statistical analysis of data for the Comp. Str. (MPa)

Attribute	Min	Max	Mean	St. Dev.
Rub. Perc.	0	100	20	21.46
W/C	0.31	0.62	0.48	0.07
Rub. Size (mm) (Min)	0	12.50	1.10	2.48
Rub. Size (mm) (Max)	0.30	30	5.72	6.22
Comp. Str. (MPa)	0.37	57.80	25.35	11.78

$$\sigma_x = f_{cts} = \frac{My}{I} \tag{8}$$

can be calculated using the Eq. (8). Here "*M*" is the moment, "*y*" is the distance diameter from the neutral axis, and "*I*" is the moment of inertia.

The reference sample's bending strength in the tests was found to be 7.99 MPa (Fig. 15). Along with the other qualities examined in this study, the mechanical quality of concrete, such as compressive strength, deteriorated concurrently with the incorporation of waste rubber. Depending on the rubber ratio applied, this reduction is approximately 75%, 51%, or 45% of the respective reference values. When the flexural strength test results are compared to the compressive strength results, it is observed that the reduction is smaller for the flexural strength.

The relationship between compressive strength and cylinder splitting strength is shown in Fig. 16.

4.2 Application of FFNN to predict the compressive strength

The specifications of the development and test platform are as follows: Windows 10 operating system, Intel(R) Core(TM) i7-6700HQ 2.66 GHz, 16 GB of memory, Visual Studio 2017, and C# programming language. The parameters of the FFNN affect the quality of the solution. The momentum factor, the learning rate, and the maximum epoch number in FFNN are set to 0.8, 0.3, and 50000, respectively. Eq. (9) shows the formulation of the generated best model.

$$Y = sigmoid(sigmoid(X \times IHW + b_1) \times HOW + b_2) \tag{9}$$

Where sigmoid(.) is the activation function, and X represents the inputs. *IHW* represents the values of the weights between the input layer and the hidden layer. How represents the values of the weights between the hidden layer and output layer. b_1 and b_2 represent the values of the biases in the hidden layer, and output layer.

The dataset consists of one output and four inputs. The input and output data are Rub. Perc. (%), W/C, Rub. Size (mm) (Min), and Rub. Size (mm) (Max). Table 3 displays the statistical analysis of the data.

In the input layer, there are four neurons, and in the output layer, there is one neuron, respectively. As previously indicated, the number of neurons in the hidden layer was initially set to 2, and then increased by one up to 30. Therefore, 29 different FFNN architectures were used to determine the best model. Successively, the validation

Table 4 The weights of the hidden layer for the Comp. Str. (MPa)

IHW			
-8.22	-8.22	-8.22	-8.22
-10.64	-10.64	-10.64	-10.64
-12.38	-12.38	-12.38	-12.38
3.72	3.72	3.72	3.72
-1.61	-1.61	-1.61	-1.61
-2.44	-2.44	-2.44	-2.44
-0.22	-0.22	-0.22	-0.22
-3.25	-3.25	-3.25	-3.25
-3.19	-3.19	-3.19	-3.19
-8.79	-8.79	-8.79	-8.79
1.33	1.33	1.33	1.33

Table 5 The biases in the hidden layer and the weights and the biases in the output layer for the Comp. Str. (MPa)

b_1	HOW	b_2
-4.32	2.09	-1.96
5.15	1.13	
4.87	1.15	
-0.56	2.34	
13.43	-1.51	
-2.49	7.66	
10.95	5.39	
12.11	-4.10	
0.01	-3.89	
-1.68	20.59	
-2.81	-21.45	

Table 6 Performance of the generated FFNN model for the Comp. Str. (MPa)

Criteria	Training	Validation	Test
Instance	125	27	27
R	0.894	0.869	0.908
MAE	2.961	2.832	2.562
MSE	15.502	13.422	12.412

dataset is applied to each of the 29 models. Thus, the best model of the 29 models is found according to the minimum MSE. According to the experimental results, the best model had 11 neurons in the hidden layer. Consequently, the architecture in the best model was 4-11-1. Table 4 shows the values of the weights in the hidden layer of the best model generated. Table 5 shows the biases in the hidden layer and the weights and biases in the output layer of the best model generated.

The performance outcomes of the created model for three sub-datasets are displayed in Table 6. The collection has 179 occurrences. Using stratified sampling, the dataset is split into three portions: 70% for training, 15% for validation, and 15% for testing. This is done to safeguard the class distribution as much as possible. The correlation coefficient (R) values are 0.894 for training, 0.869 for validation, and 0.908 for testing. A correlation that is close to 1 suggests a very strong association, whereas a coefficient that is close to 0 indicates a very weak relationship. The larger the coefficient, the stronger the relationship (Bachman 2004). There is a strong association because the R values for the training, validation, and test, are all close to one. For the training, validation, and test sets, the MAE values are 2.961, 2.832, and 2.562, respectively. For the training, validation, and test datasets, the MSE values are 15.502, 13.422, and 12.412, respectively. Lower MSE and MAE indicate more accurate predictions. These findings show that the developed FFNN model performs well and makes correct predictions for the Comp. Str. (MPa).

The regression plots of the generated FFNN model are shown in Fig. 17. The predictive performance of the proposed FFNN model is satisfactory according to the plots of the training, validation, test, and all data.

Fig. 18 displays the error histogram of the constructed FFNN model. It offers more evidence that the artificial neural network is operating efficiently. The blue, green, and red regions represent training, validation, and test data, respectively. The majority of the data are zero-error data, so it makes sense to examine the anomalies to determine if the data are suspect or if those data points are unique. If the anomalies are genuine data points distinct from the remaining data, the network extrapolates these points. (Yadav *et al.* 2015). The density in the error histogram is around 0, as depicted in Fig. 18. Therefore, the prediction success of the generated FFNN model is very high.

4.3 Application of FFNN to predict the Spl. Ten. Str. (MPa)

There are four inputs and one output in the dataset. The input data are Rub. Perc. (%), W/C Rub. Size (mm) (Min), and Rub. Size (mm) (Max): output data are Spl. Ten. Str. (MPa). Table 7 shows the statistical analysis of the data.

In the input and output layers, there are four and one neurons, respectively. As previously indicated, the number of neurons in the hidden layer was initially set to 2 and then increased by one up to 30. Therefore, 29 different FFNN architectures were used to determine the best model. Then successively, the validation dataset is applied to each of the 29 models. Thus, the best model among the 29 models is found according to the minimum MSE. According to the experimental results, the best model had 22 neurons in the hidden layer. Consequently, the architecture of the best model was 4-22-1. Table 8 shows the values of weights in the hidden layer of the best model generated. Table 9 shows the biases in the hidden layer and the weights and biases in the output layer of the best-generated model.

The performance outcomes of the created model for three sub-datasets are displayed in Table 10. The collection has 69 examples. Using stratified sampling, the dataset is split into three portions: 70% for training, 15% for validation, and 15% for testing. This is done to safeguard

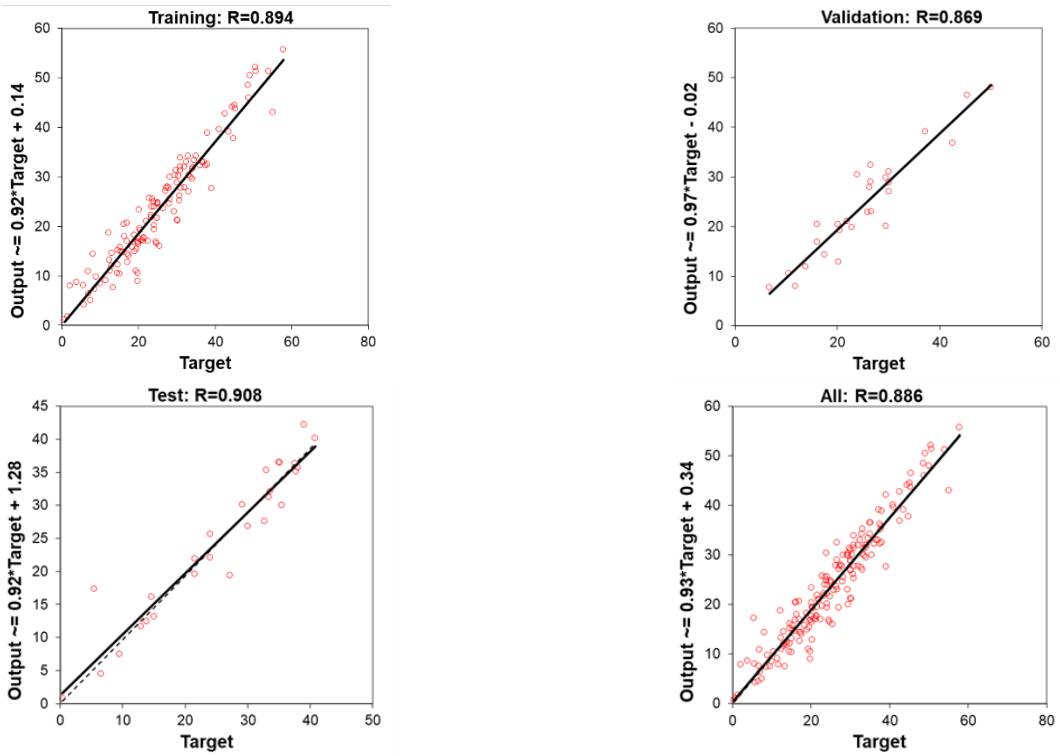


Fig. 17 The regression results of the training, validation, test, and all data for the Comp. Str. (MPa)

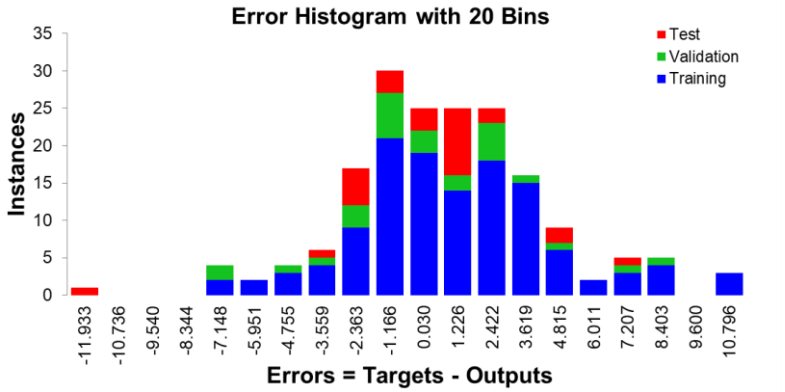


Fig. 18 The error histogram for the Comp. Str. (MPa)

Table 7 Statistical analysis of data for the Spl. Ten. Str. (MPa)

Attribute	Min	Max	Mean	St. Dev.
Rub. Perc.	0	100	24.77	28.33
W/C	0.30	0.62	0.45	0.10
Rub. Size (mm) (Min)	0	15	1.20	2.82
Rub. Size (mm) (Max)	0.85	25	5.14	4.90
Spl. Ten. Str. (MPa)	0.22	7.50	2.72	1.45

the class distribution as much as possible. For the training, validation, and testing, the correlation coefficient (R) values are 0.912, 0.931, and 0.896, respectively. There is a very strong association in the model because the R values for the training, validation, and test are all very close to one. For the training, validation, and testing, the MAE values are 0.237, 0.308, and 0.273, respectively. For the training, validation, and test sets, the MSE values are 0.189, 0.139, and 0.121, respectively. These findings show that the developed FFNN model performs very well and makes correct predictions for the Spl. Ten. Str. (Tensile Strength in Megapascals) (MPa).

The regression plots of the generated FFNN model are shown in Fig. 19. According to the plots of the training, validation, test, and all data, the prediction performance of the proposed FFNN model is good.

Fig. 20 displays the error histogram for the developed FFNN model. It offers more evidence that the artificial neural network is operating effectively. It shows anomalies. The blue, green, and red areas, respectively, represent the training, validation, and test data. According to Fig. 20, the density of the error histogram is close to zero. As a result, the FFNN model has a high predictive accuracy.

Table 8 The weights of the hidden layer for the Spl. Ten. Str. (MPa)

IHW			
-2.60	-1.22	0.25	-0.56
-5.82	-5.12	-1.35	-3.50
-1.08	-1.20	0.24	-0.75
1.35	-0.07	-0.60	-2.63
-13.48	-0.56	-15.07	-2.84
-1.08	-3.79	1.88	3.80
-0.86	-0.41	-0.57	-0.49
0.14	-2.27	1.43	0.53
-3.98	-1.92	-4.23	-2.88
3.70	3.26	0.07	-10.87
-0.51	-1.95	0.54	-0.73
-1.21	-0.84	-1.33	-0.33
0.39	-1.58	0.20	0.21
0.38	-2.24	1.34	-0.38
-1.03	0.46	-0.24	-0.31
-3.77	-2.55	0.97	-2.04
2.93	12.37	-4.24	8.88
-2.52	5.55	-5.59	-0.83
-0.77	-1.79	0.61	1.80
0.43	-0.95	0.00	-0.80
9.71	-4.45	2.67	-6.76
2.26	6.26	1.07	5.84

Table 9 The biases in the hidden layer and the weights and the biases in the output layer for the Spl. Ten. Str. (MPa)

b_1	HOW	b_2
-3.02	0.58	0.33
-0.91	3.34	
-2.91	0.31	
-3.49	-0.42	
-1.77	6.31	
-1.84	-1.54	
-3.23	0.32	
-3.10	-0.72	
-2.46	2.29	
-2.94	-2.76	
-2.71	0.05	
-3.13	0.31	
-3.15	-0.44	
-2.98	-0.52	
-3.53	0.44	
-2.28	1.83	
-8.80	-3.33	
-5.68	4.49	
-2.87	-1.12	
-3.16	-0.12	
-1.25	-1.84	
-7.18	4.87	

4.4 Application of FFNN to predict the Flex. Str. (MPa)

There are four inputs and one output in the dataset. The input data are Rub. Perc. (%), W/C, Rub. Size (mm) (Min), and Rub. Size (mm) (Max), the output datum is Flex. Ten. Str. (MPa). Table 11 presents the statistical evaluation of the data.

In the input and output layers, there are four and one neurons, respectively. As previously indicated, the number of neurons in the hidden layer was initially set to 2 and then increased by one up to 30. Therefore, 29 different FFNN architectures were used to determine the best model. Then successively, the validation dataset is applied to each of the 29 models. Thus, the best model among the 29 models is found according to the minimum MSE. According to the experimental results, the best model had 11 neurons in the hidden layer. Consequently, the architecture in the best model was 4-11-1. Table 12 shows the values of weights in the hidden layer of the generated best model. Table 13 shows the biases in the hidden layer, and the weights and biases in the output layer of the generated best model.

The performance outcomes of the created model for three sub-datasets are displayed in Table 14. The collection has 98 cases. Using stratified sampling, the dataset is split into three portions: 70% for training, 15% for validation, and 15% for testing. This is done to safeguard the class distribution as much as feasible. For the training, validation, and test sets, the correlation coefficient (R) values are 0.996, 0.991, and 0.931, respectively. There is a very strong association in the model because the R values in the training, validation, and test sets are each close to one. For the training set, validation set, and test set, the MAE values are 0.067, 0.125, and 0.257, respectively. The values of the MSE are 0.009, 0.031, and 0.153 for the training, validation, and test datasets, respectively. According to these results, the generated FFNN model performs effectively and accurately predicts Flex. Str. (MPa).

Table 10 Performance of the generated FFNN model for the Spl. Ten. Str. (MPa)

Criteria	Training	Validation	Test
Instance	48	10	11
R	0.912	0.931	0.896
MAE	0.237	0.308	0.273
MSE	0.191	0.139	0.121

Fig. 21 displays the regression graphs produced by the constructed FFNN model. According to the plots of all the data: training, validation, and test sets, the suggested FFNN model's prediction performance is strong.

Fig. 22 displays the error histogram for the FFNN model. It offers more evidence that the artificial neural network is operating effectively. It shows anomalies. The blue, green, and red areas, respectively, represent the

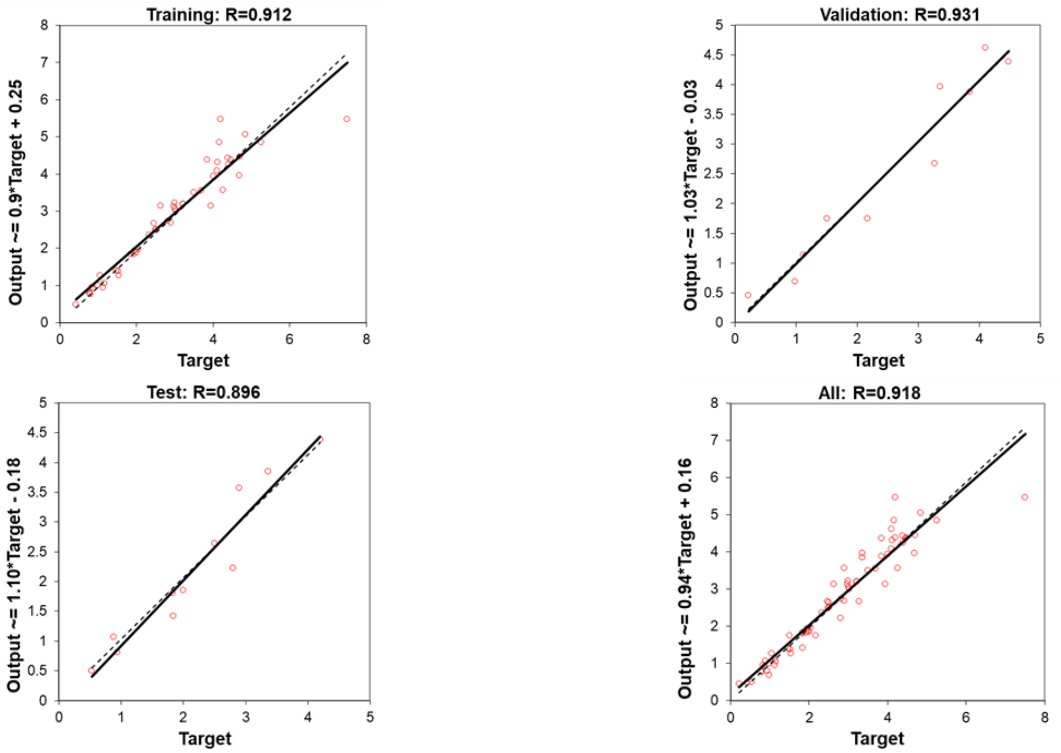


Fig. 19 The regression results of the training, validation, test, and all data for the Spl. Ten. Str. (MPa)

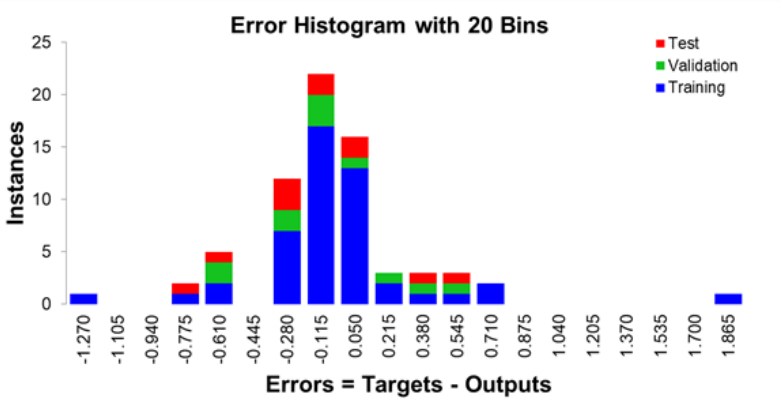


Fig. 20 The error histogram for the Spl. Ten. Str. (MPa)

training, validation, and test data. According to Fig. 22, the density of the error histogram is close to zero. As a result, the developed FFNN model has a very high prediction success rate.

5. Scanning electron microscope (SEM) analysis

SEM produces high-resolution images, allowing the examination of small structures and details in the sample. The Interface Transition Zone (ITZ) refers to the region in a composite material where two different materials or phases meet and mix, often causing changes in the mechanical, thermal, and chemical properties of the material. The interaction between aggregate and cement paste typically occurs at the interface region in concrete structures. ITZ is clearly visible in Fig. 23(a). According to Zhai *et al.* (2023), the adhesion between the rubber particles and the cement matrix becomes very weak, and segregation (ITZ) occurs. The interface becomes the weakest area and is easily damaged under external loads. Many micro-cracks start and expand rapidly due to the impact load, especially around the rubber particles (Najim and Hall 2010). In addition, Fig. 23(b) shows the formation of microcracks and larger pores. These are disadvantages regarding the mechanical performance of concrete. The amorphous phase calcium silicate hydrate (C-S-H) is characterized by poorly ordered crystals (Kim *et al.* 2015). In Fig. 23(c), the C-S-H construction draws attention. Fig. 19(c) also shows ettringite formation. Ettringite is commonly found in hydrothermal veins, mining works, as well as in cementitious environments. It is also considered an important mineral in the cement industry, as it is formed as a hydration product during the setting and hardening of

Table 11 Statistical analysis of data for the Flex Str. (MPa)

Attribute	Min	Max	Mean	St. Dev.
Rub. Perc.	0	100	24.51	27.14
W/C	0.31	0.54	0.44	0.06
Rub. Size (mm) (Min)	0	12.50	1.63	3.03
Rub. Size (mm) (Max)	0.50	20	5.64	4.53
Flex. Str. (MPa)	0.64	7.50	3.97	1.61

Table 12 The weights of the hidden layer for the Flex. Str. (MPa)

IHW			
-3.60	1.51	-0.73	-13.69
-1.74	-4.17	-0.23	-2.08
3.22	7.69	-7.88	-16.44
-2.28	-0.73	-0.71	-1.21
-2.46	-5.11	-0.01	-3.47
-3.02	-0.28	0.49	-1.94
0.16	-7.00	8.26	-15.22
1.42	1.83	-4.04	-5.54
0.63	-1.59	-0.38	-1.05
2.18	-7.55	13.46	-10.54
0.77	16.47	2.48	-5.36

Table 13 The biases in the hidden layer and the weights and the biases in the output layer for the Flex. Str. (MPa)

b_1	HOW	b_2
-0.81	6.53	1.09
-1.38	1.81	
-4.01	-4.79	
-0.70	-1.87	
-0.45	2.55	
-1.73	-1.36	
7.06	6.02	
1.21	-4.06	
-1.78	-0.94	
4.27	-5.09	
-12.88	4.94	

Portland cement (Zeybek *et al.* 2022). Ettringite formation can affect the performance and durability of cementitious materials as it can cause the material to expand and crack (Sun *et al.* 2021).

6. Conclusions

This study examined the mechanical properties of concrete produced, by incorporating waste rubber fibers by weight. Various proportions of waste tires were utilized. Different approaches were proposed to compute the capacities of concrete with waste rubber obtained from used tires.

Table 14 Performance of the generated FFNN model for the Flex. Str. (MPa)

Criteria	Training	Validation	Test
Instance	69	15	14
R	0.996	0.991	0.931
MAE	0.067	0.125	0.257
MSE	0.009	0.031	0.153

• The use of waste rubber enhances the workability of concrete by affecting the water-cement interaction. Considering the slump values, the lowest value was in the reference sample, the highest value was obtained in the mixture produced using 15% rubber.

• The use of waste tires caused a decrease in the concrete unit weight. The unit volume weight decreases in parallel with the increase in the use of the tire ratio. The concrete with the lowest density was obtained when 15% waste rubber was used.

• The decrease in unit volume weight will have a positive effect by reducing the loads directly related to the weight of the building, such as effects like earthquakes, when concrete produced using waste rubber is employed as a structural material.

• High compressive strength is the most important mechanical property of concrete. The use of waste rubber has reduced the compressive strength of concrete, and this decrease becomes more pronounced as the amount of waste rubber increases. This result shows that if concrete produced using waste rubber is to be used as carrier concrete, innovative methods that do not reduce the compressive strength should be employed.

• Concrete is a material with low tensile strength. When both the cylinder split test and the beam bending tensile test results are examined, the use of waste rubber, caused a decrease in the tensile strength of the concrete. The decrease obtained in both tensile tests is not as much as the decrease in compressive strength because rubber is used as a form of fiber.

• If rubberized concrete is used as a carrier in a real structure, the decrease in unit weight will reduce the overall weight of the building, and this will cause a decrease in forces that are linearly related to the building's weight, such as those exerted by earthquakes.

• In this study, three different predictive models based on the feed-forward neural network were developed to predict the compressive stress (MPa), the splitting tensile strength (MPa), and the flexural strength (MPa). In the experiments, the effectiveness of the predictive models was verified on three data sets. The values of the weights in FFNN were also presented. In conclusion, the experimental results indicate that the proposed models are successful in predicting the compressive stress, the Spl. Ten. Str. (MPa), and the Flex. Str. (MPa) with an acceptable degree of accuracy.

• Although the formation of microcracks, pores, and ettringites in SEM analysis seems to be a disadvantage, the formation of C-S-H gels as a result of hydration shows that

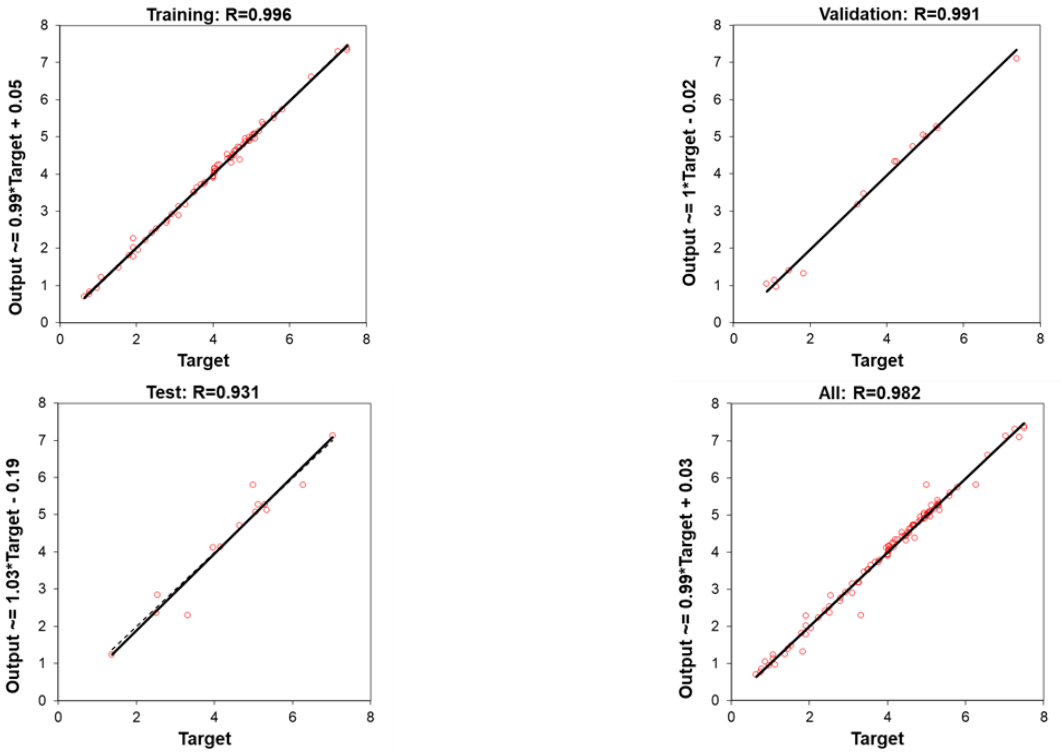


Fig. 21 The regression results of the training, validation, test, and all data for the Flex. Str. (MPa)

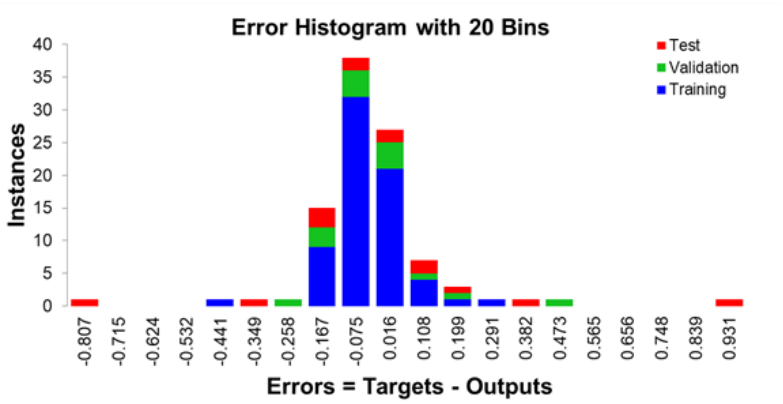


Fig. 22 The error histogram for the Flex. Str. (MPa)

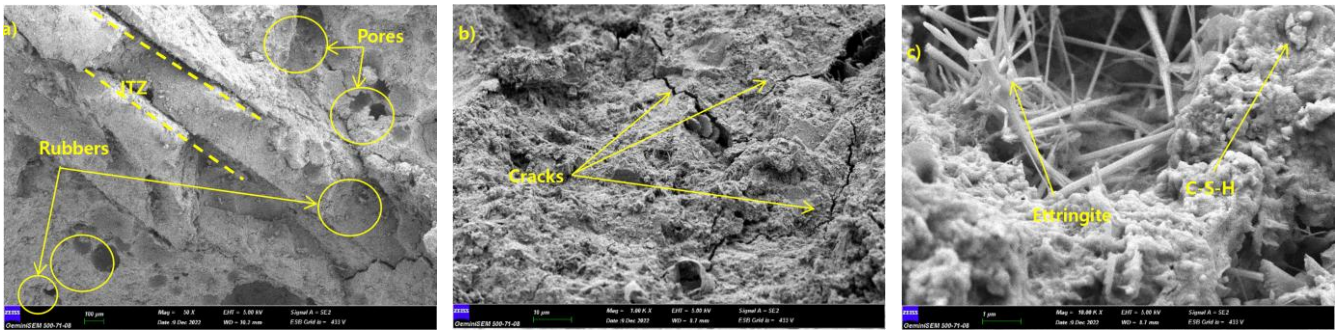


Fig. 23 SEM analysis

good bonding is formed in the structure.

References

Abendeh, R., Ahmad, H.S. and Hunaiti, Y.M. (2016), "Experimental studies on the behavior of concrete-filled steel tubes incorporating crumb rubber", *J. Constr. Steel Res.*, **122**, 251-260. https://doi.org/10.1016/j.jcsr.2016.03.022.

Ahmad, J., Zhou, Z., Majdi, A., Alqurashi, M. and Deifalla, A.F.

(2022), "Overview of concrete performance made with waste rubber tires: A step toward sustainable concrete", *Mater. (Basel)*, **15**(16), 5518. https://doi.org/10.3390/ma15165518.

Aiello, M.A. and Leuzzi, F. (2010), "Waste tyre rubberized concrete: properties at fresh and hardened state", *Waste Manag.* **30**(8-9), 1696-1704. https://doi.org/10.1016/j.wasman.2010.02.005

Al-Tayeb, M.M., Abu Bakar, B.H., Akil, H.M. and Ismail, H. (2012), "Performance of Rubberized and Hybrid Rubberized Concrete Structures under Static and Impact Load Conditions", *Exper. Mech.*, **53**(3), 377-384. https://doi.org/10.1007/s11340-012-9651-z.

Aliabdo, A.A., Abd Elmoaty, A.E.M. and AbdElbaset, M.M. (2015), "Utilization of waste rubber in non-structural applications", *Constr. Build. Mater.*, **91**, 195-207. https://doi.org/10.1016/j.conbuildmat.2015.05.080.

Amiri, M., Hatami, F. and Golafshani, E.M. (2021), "Evaluating the synergic effect of waste rubber powder and recycled concrete aggregate on mechanical properties and durability of concrete", *Case Stud. Constr. Mater.*, **15**, e00639. https://doi.org/10.1016/j.cscm.2021.e00639.

Atahan, A.O. and Yücel, A.Ö. (2012), "Crumb rubber in concrete: Static and dynamic evaluation", *Constr. Build. Mater.*, **36**, 617-622. https://doi.org/10.1016/j.conbuildmat.2012.04.068.

Bachman, L.F. (2004), *Statistical Analyses for Language Assessment Book*, Cambridge University Press, Cambridge, UK.

Batayneh, M.K., Marie, I. and Asi, I. (2008), "Promoting the use of crumb rubber concrete in developing countries", *Waste Manag.* **28**(11), 2171-2176. https://doi.org/10.1016/j.wasman.2007.09.035.

Beiram, A.A.H. and Al-Mutairee, H.M.K. (2022), "Effect of using waste rubber as partial replacement of coarse aggregate on torsional strength of square reinforced concrete beam", *Int. J. Eng.*, **35**(2), 397-405. https://doi.org/10.5829/IJE.2022.35.02B.16.

Bignozzi, M.C. and Sandrolini, F. (2006), "Tyre rubber waste recycling in self-compacting concrete", *Cement Concrete Res.*, **36**(4), 735-739. https://doi.org/10.1016/j.cemconres.2005.12.011.

Bisht, K. and Ramana, P.V. (2017), "Evaluation of mechanical and durability properties of crumb rubber concrete", *Constr. Build. Mater.*, **155**, 811-817. https://doi.org/10.1016/j.conbuildmat.2017.08.131.

Bravo, M. and de Brito, J. (2012), "Concrete made with used tyre aggregate: Durability-related performance", *J. Clean. Prod.*, **25**, 42-50. https://doi.org/10.1016/j.jclepro.2011.11.066.

Bušić, R., Miličević, I., Šipoš, T.K. and Strukar, K. (2018), "Recycled rubber as an aggregate replacement in self-compacting concrete—Literature overview", *Mater.*, **11**(9), 1729. https://doi.org/10.3390/ma11091729.

Cao, Y., Li, L., Liu, M. and Wu, Y. (2021), "Mechanical behavior of FRP confined rubber concrete under monotonic and cyclic loading", *Compos. Struct.*, **272**, 114205. https://doi.org/10.1016/j.compstruct.2021.114205.

Elchalakani, M. (2015), "High strength rubberized concrete containing silica fume for the construction of sustainable road side barriers", *Struct.*, **1**, 20-38. https://doi.org/10.1016/j.istruc.2014.06.001.

Elchalakani, M., Aly, T. and Abu-Aisheh, E. (2016), "Mechanical properties of rubberised concrete for road side barriers", *Aust. J. Civil Eng.*, **14**(1), 1-12. https://doi.org/10.1080/14488353.2015.1092631.

Ferdous, W., Manalo, A., Al Ajarmeh, O.S., Zhuge, Y., Mohammed, A.A., Bai, Y., Aravinthan, T. and Schubel, P. (2021), "Bending and shear behaviour of waste rubber concrete-filled FRP tubes with external flanges", *Polym. (Basel)*, **13**(15), 2500. https://doi.org/10.3390/polym13152500.

Gesoglu, M., Güneyisi, E., Hansu, O., İpek, S. and Asaad, D.S. (2015), "Influence of waste rubber utilization on the fracture and steel-concrete bond strength properties of concrete", *Constr. Build. Mater.*, **101**, 1113-1121. https://doi.org/10.1016/j.conbuildmat.2015.10.030.

Grinys, A., Sivilevičius, H. and Daukšys, M. (2012), "Tyre rubber additive effect on concrete mixture strength", *J. Civil Eng. Manag.*, **18**(3), 393-401. https://doi.org/10.3846/13923730.2012.693536.

Gupta, T., Chaudhary, S. and Sharma, R.K. (2014), "Assessment of mechanical and durability properties of concrete containing waste rubber tire as fine aggregate", *Constr. Build. Mater.*, **73**, 562-574. https://doi.org/10.1016/j.conbuildmat.2014.09.102.

Gupta, T., Siddique, S., Sharma, R.K. and Chaudhary, S. (2019), "Behaviour of waste rubber powder and hybrid rubber concrete in aggressive environment", *Constr. Build. Mater.*, **217**, 283-291. https://doi.org/10.1016/j.conbuildmat.2019.05.080.

Guru Prasad, M., Yadav Golla, S., Prabhanjan, N., Siva Krishna, A. and Alok, G. (2021), "Mechanical properties of rubberized concrete using truck scrap rubber", *Mater. Today: Proc.*, **39**, 849-854. https://doi.org/10.1016/j.matpr.2020.10.358.

Güneyisi, E. (2009), "Fresh properties of self-compacting rubberized concrete incorporated with fly ash", *Mater. Struct.*, **43**(8), 1037-1048. https://doi.org/10.1617/s11527-009-9564-1.

Ganjian, E., Khorami, M. and Maghsoudi, A.A. (2009), "Scrap-tyre-rubber replacement for aggregate and filler in concrete", *Constr. Build. Mater.*, **23**(5), 1828-1836. https://doi.org/10.1016/j.conbuildmat.2008.09.020.

Gülcü, Ş. (2020), "Training of the artificial neural networks using states of matter search algorithm", *Int. J. Intell. Syst. Appl. Eng.*, **8**(3), 131-136. https://doi.org/10.18201/ijisae.2020363532.

Gülcü, Ş. (2022a), "An improved animal migration optimization algorithm to train the feed-forward artificial neural networks", *Arab. J. Sci. Eng.*, **47**(8), 9557-9581. https://doi.org/10.1007/s13369-021-06286-z.

Gülcü, Ş. (2022b), "Training of the feed forward artificial neural networks using dragonfly algorithm", *Appl. Soft Comput.*, **124**, 109023. https://doi.org/10.1016/j.asoc.2022.109023.

Habib, A. and Yildirim, U. (2021), "Prediction of the dynamic properties in rubberized concrete", *Comput. Concrete*, **27**(3), 185-197. https://doi.org/10.12989/cac.2021.27.3.185.

Han, Q.H., Xu, J., Xing, Y. and Li, Z.L. (2015), "Static push-out test on steel and recycled tire rubber-filled concrete composite beams", *Steel Compos. Struct.*, **19**(4), 843-860. https://doi.org/10.12989/scs.2015.19.4.843.

Han, Q.H., Wang, Y.H., Xu, J. and Xing, Y. (2016), "Fatigue behavior of stud shear connectors in steel and recycled tyre rubber-filled concrete composite beams", *Steel Compos. Struct.*, **22**(2), 353-368. https://doi.org/10.12989/scs.2016.22.2.353.

Herrera-Sosa, E.S., Martínez-Barrera, G., Barrera-Díaz, C. and Cruz-Zaragoza, E. (2014), "Waste tire particles and gamma radiation as modifiers of the mechanical properties of concrete", *Adv. Mater. Sci. Eng.*, **2014**, 1-7. https://doi.org/10.1155/2014/327856.

Hernandez-Olivares, F., Barluenga, G., Bollati, M. and Witoszek, B. (2002), "Static and dynamic behaviour of recycled tyre rubber-filled concrete", *Cement Concrete Res.*, **32**(10), 1587-1596. https://doi.org/10.1016/S0008-8846(02)00833-5.

Hesami, S., Salehi Hikouei, I. and Emadi, S.A.A. (2016), "Mechanical behavior of self-compacting concrete pavements incorporating recycled tire rubber crumb and reinforced with polypropylene fiber", *J. Clean. Prod.*, **133**, 228-234. https://doi.org/10.1016/j.jclepro.2016.04.079.

Ince, C., Shehata, B.M.H., Derogar, S. and Ball, R.J. (2022), "Towards the development of sustainable concrete incorporating waste tyre rubbers: A long-term study of physical, mechanical & durability properties and environmental impact",

J. Clean. Prod., **334**, 130223. https://doi.org/10.1016/j.jclepro.2021.130223.

Islam, M.M.U., Li, J., Wu, Y.F., Roychand, R. and Saberian, M. (2022), "Design and strength optimization method for the production of structural lightweight concrete: An experimental investigation for the complete replacement of conventional coarse aggregates by waste rubber particles", *Resour. Conserv. Recycl.*, **184**, 106390. https://doi.org/10.1016/j.resconrec.2022.106390.

Ismail, M.K. and Hassan, A.A.A. (2016), "Use of metakaolin on enhancing the mechanical properties of self-consolidating concrete containing high percentages of crumb rubber", *J. Clean. Prod.*, **125**, 282-295. https://doi.org/10.1016/j.jclepro.2016.03.044.

Jokar, F., Khorram, M., Karimi, G. and Hataf, N. (2019), "Experimental investigation of mechanical properties of crumbed rubber concrete containing natural zeolite", *Constr. Build. Mater.*, **208**, 651-658. https://doi.org/10.1016/j.conbuildmat.2019.03.063.

Kazmi, S.M.S., Munir, M.J. and Wu, Y.F. (2021), "Application of waste tire rubber and recycled aggregates in concrete products: A new compression casting approach", *Resour. Conserv. Recycl.*, **167**, 105353. https://doi.org/10.1016/j.resconrec.2020.105353.

Ke, X., Xiang, W. and Ye, C. (2022), "Mechanical properties and damage constitutive model of self-compacting rubberized concrete", *Comput. Concrete*, **30**(4), 257-267. https://doi.org/10.12989/cac.2022.30.4.257.

Khaloo, A.R., Dehestani, M. and Rahmatabadi, P. (2008), "Mechanical properties of concrete containing a high volume of tire-rubber particles", *Waste Manag*. **28**(12), 2472-2482. https://doi.org/10.1016/j.wasman.2008.01.015.

Khern, Y.C., Paul, S.C., Kong, S.Y., Babafemi, A.J., Anggraini, V., Miah, M.J. and Šavija, B. (2020), "Impact of chemically treated waste rubber tire aggregates on mechanical, durability and thermal properties of concrete", *Front. Mater.*, **7**, 90. https://doi.org/10.3389/fmats.2020.00090.

Khaloo, A.R., Dehestani, M. and Rahmatabadi, P. (2008), "Mechanical properties of concrete containing a high volume of tire-rubber particles", *Waste Manag.*, **28**(12), 2472-2482. https://doi.org/10.1016/j.wasman.2008.01.015.

Kim, J., Yi, C. and Zi, G. (2015), "Waste glass sludge as a partial cement replacement in mortar", *Constr. Build. Mater.*, **75**, 242-246. https://doi.org/10.1016/j.conbuildmat.2014.11.007.

Li, L., Ruan, S. and Zeng, L. (2014), "Mechanical properties and constitutive equations of concrete containing a low volume of tire rubber particles", *Constr. Build. Mater.*, **70**, 291-308. https://doi.org/10.1016/j.conbuildmat.2014.07.105.

Ling, T.C. (2011), "Prediction of density and compressive strength for rubberized concrete blocks", *Constr. Build. Mater.*, **25**(11), 4303-4306. https://doi.org/10.1016/j.conbuildmat.2011.04.074.

Liu, F., Zheng, W., Li, L., Feng, W. and Ning, G. (2013), "Mechanical and fatigue performance of rubber concrete", *Constr. Build. Mater.*, **47**, 711-719. https://doi.org/10.1016/j.conbuildmat.2013.05.055,

Lv, J., Zhou, T., Du, Q. and Wu, H. (2015), "Effects of rubber particles on mechanical properties of lightweight aggregate concrete", *Constr. Build. Mater.*, **91**, 145-149. https://doi.org/10.1016/j.conbuildmat.2015.05.038.

Najim, K.B. and Hall, M.R. (2012), "Mechanical and dynamic properties of self-compacting crumb rubber modified concrete", *Constr. Build. Mater.*, **27**(1), 521-530. https://doi.org/10.1016/j.conbuildmat.2011.07.013.

Najim, K.B. and Hall, M.R. (2013), "Crumb rubber aggregate coatings/pre-treatments and their effects on interfacial bonding, air entrapment and fracture toughness in self-compacting rubberised concrete (SCRC)", *Mater. Struct.*, **46**(12), 2029-2043. https://doi.org/10.1617/s11527-013-0034-4.

Najim, K. and Hall, M. (2010), "A review of the fresh/hardened properties and applications for plain-(PRC) and self-compacting rubberised concrete (SCRC)", *Constr. Build. Mater.*, **24**(11), 2043-2051. https://doi.org/10.1016/j.conbuildmat.2010.04.056.

Navarro, F., Partal, P., Martínez-Boza, F. and Gallegos, C. (2005), "Influence of crumb rubber concentration on the rheological behavior of a crumb rubber modified bitumen", *Energy Fuels*, **19**(5), 1984-1990. https://doi.org/10.1021/ef049699a.

Raffoul, S., Garcia, R., Pilakoutas, K., Guadagnini, M. and Medina, N.F. (2016), "Optimisation of rubberised concrete with high rubber content: An experimental investigation", *Constr. Build. Mater.*, **124**, 391-404. https://doi.org/10.1016/j.conbuildmat.2016.07.054.

Reda Taha, M.M., El-Dieb, A.S., Abd El-Wahab, M.A. and Abdel-Hameed, M.E. (2008), "Mechanical, fracture, and microstructural investigations of rubber concrete", *J. Mater. Civil Eng.*, **20**(10), 640-649. https://doi.org/10.1061/(ASCE)0899-1561(2008)20:10(640).

Rezaifar, O., Hasanzadeh, M. and Gholhaki, M. (2016), "Concrete made with hybrid blends of crumb rubber and metakaolin: Optimization using Response Surface Method", *Constr. Build. Mater.*, **123**, 59-68. https://doi.org/10.1016/j.conbuildmat.2016.06.047.

Roychand, R., Gravina, R.J., Zhuge, Y., Ma, X., Youssf, O. and Mills, J.E. (2020), "A comprehensive review on the mechanical properties of waste tire rubber concrete", *Constr. Build. Mater.*, **237**, 117651. https://doi.org/10.1016/j.conbuildmat.2019.117651.

Stallings, K.A., Durham, S.A. and Chorzepa, M.G. (2019), "Effect of cement content and recycled rubber particle size on the performance of rubber-modified concrete", *Int. J. Sustainab. Eng.*, **12**(3), 189-200. https://doi.org/10.1080/19397038.2018.1505971.

Su, H., Yang, J., Ling, T.C., Ghataora, G.S. and Dirar, S. (2015), "Properties of concrete prepared with waste tyre rubber particles of uniform and varying sizes", *J. Clean. Prod.*, **91**, 288-296. https://doi.org/10.1016/j.jclepro.2014.12.022.

Sun, J., Wang, Y., Liu, S., Dehghani, A., Xiang, X., Wei, J. and Wang, X. (2021), "Mechanical, chemical and hydrothermal activation for waste glass reinforced cement", *Constr. Build. Mater.*, **301**, 124361. https://doi.org/10.1016/j.conbuildmat.2021.124361.

Sofi, A. (2018), "Effect of waste tyre rubber on mechanical and durability properties of concrete - A review", *Ain Shams Eng. J.*, **9**(4), 2691-2700. https://doi.org/10.1016/j.asej.2017.08.007.

Stallings, K.A., Durham, S.A. and Chorzepa, M.G. (2018), "Effect of cement content and recycled rubber particle size on the performance of rubber-modified concrete", *Int. J. Sustainab. Eng.*, **12**(3), 189-200. https://doi.org/10.1080/19397038.2018.1505971.

Thomas, B.S., Gupta, R.C., Kalla, P. and Cseteneyi, L. (2014), "Strength, abrasion and permeation characteristics of cement concrete containing discarded rubber fine aggregates", *Constr. Build. Mater.*, **59**, 204-212. https://doi.org/10.1016/j.conbuildmat.2014.01.074.

Topçu, İ.B. and Demir, A. (2007), "Durability of rubberized mortar and concrete", *J. Mater. Civil Eng.*, **19**(2), 173-178. https://doi.org/10.1061/(ASCE)0899-1561(2007)19:2(173).

Toutanji, H.A. (1996), "The use of rubber tire particles in concrete to replace mineral aggregates", *Cement Concrete Compos.*, **18**(2), 135-139. https://doi.org/10.1016/0958-9465(95)00010-0.

Turatsinze, A., Bonnet, S. and Granju, J.L. (2007), "Potential of rubber aggregates to modify properties of cement based-mortars: Improvement in cracking shrinkage resistance", *Constr. Build. Mater.*, **21**(1), 176-181. https://doi.org/10.1016/j.conbuildmat.2005.06.036.

Turatsinze, A. and Garros, M. (2008), "On the modulus of elasticity and strain capacity of Self-Compacting Concrete incorporating rubber aggregates", *Resour. Conserv. Recycl.*, **52**(10), 1209-1215. https://doi.org/10.1016/j.resconrec.2008.06.012.

Turki, M., Bretagne, E., Rouis, M.J. and Quéneudec, M. (2009), "Microstructure, physical and mechanical properties of mortar-rubber aggregates mixtures", *Constr. Build. Mater.*, **23**(7), 2715-2722. https://doi.org/10.1016/j.conbuildmat.2008.12.019.

Valente, M. and Sibai, A. (2019), "Rubber/crete: Mechanical properties of scrap to reuse tire-derived rubber in concrete, A review", *J. Appl. Biomat. Funct. Mater.*, **17**(1S), 2280800019835486. https://doi.org/10.1177/2280800019835.

Xu, J., Niu, X. and Yao, Z. (2021), "Mechanical properties and acoustic emission data analyses of crumb rubber concrete under biaxial compression stress states", *Constr. Build. Mater.*, **298**, 123778. https://doi.org/10.1016/j.conbuildmat.2021.123778.

Youssf, O., Hassanli, R. and Mills, J.E. (2017), "Mechanical performance of FRP-confined and unconfined crumb rubber concrete containing high rubber content", *J. Build. Eng.*, **11**, 115-126. https://doi.org/10.1016/j.jobe.2017.04.011.

Yung, W.H., Yung, L.C. and Hua, L.H. (2013), "A study of the durability properties of waste tire rubber applied to self-compacting concrete", *Constr. Build. Mater.*, **41**, 665-672. https://doi.org/10.1016/j.conbuildmat.2012.11.019.

Záleská, M., Pavlík, Z., Čítek, D., Jankovský, O. and Pavlíková, M. (2019), "Eco-friendly concrete with scrap-tyre-rubber-based aggregate - Properties and thermal stability", *Constr. Build. Mater.*, **225**, 709-722. https://doi.org/10.1016/j.conbuildmat.2019.07.168.

Yadav, A.K., Malik, H. and Mittal, A. (2015), "Artificial neural network fitting tool based prediction of solar radiation for identifying solar power potential", *J. Electr. Eng.*, **15**(2), 25-29.

Zeybek, Ö., Özkılıç, Y.O., Çelik, A.İ., Deifalla, A.F., Ahmad, M. and Sabri Sabri, M.M. (2022), "Performance evaluation of fiber-reinforced concrete produced with steel fibers extracted from waste tire", *Front. Mater.*, **9**, 1057128. https://doi.org/10.3389/fmats.2022.1057128

Zhai, S., Zhou, X., Zhang, Y., Pang, B., Liu, G., Zhang, L., Yang, L., Liu, Z. and Liu, L. (2023), "Effect of multifunctional modification of waste rubber powder on the workability and mechanical behavior of cement-based materials", *Constr. Build. Mater.*, **363**, 129880. https://doi.org/10.1016/j.conbuildmat.2022.129880.

Zheng, L., Huo, X.S. and Yuan, Y. (2008), "Experimental investigation on dynamic properties of rubberized concrete", *Constr. Build. Mater.*, **22**(5), 939-947. https://doi.org/10.1016/j.conbuildmat.2007.03.005.

CC